

A HIL simulator of Flexible-link Mechanisms

Paolo Boscariol · Alessandro Gasparetto ·
Vanni Zanutto

Received: 7 June 2010 / Accepted: 18 January 2011
© Springer Science+Business Media B.V. 2011

Abstract The aim of this paper is to develop a Hardware-In-the-Loop (HIL) simulator of flexible-link mechanisms. The core of the simulator is a highly accurate FEM nonlinear dynamic model of planar mechanisms. The accuracy of the proposed simulator is proved by comparing the response of the virtual model with the response of the real mechanism by using the same real controller. Results are provided by the use of classical controllers real-time capability of the dynamic model is guaranteed by a symbolic manipulation of the equations that describe the mechanism, in order to avoid the numerical inversion of the large mass matrix of the system. This HIL simulator is a valuable tool for the tuning of closed-loop control strategies for this class of mechanisms, since it allows to reduce the safety risks and the time needed to fine tune the real-time controller parameters.

Keywords Mechanical vibrations · Hardware-In-the-Loop ·
Flexible-link mechanism

1 Introduction

Flexible-link robot manipulators show many advantages over their rigid counterparts: they are lighter in weight, have faster manipulation speed, lower power consumption and need smaller actuators. Moreover, they are safer to work, have a less overall cost and higher payload with respect to the robot weight ratio. However, the control of flexible-link manipulators is quite challenging, especially in case of high operative speed. The resulting vibration can lead to poor positioning performance, to instability and mechanical breakage. For this reason from the 70's a great deal of

P. Boscariol · A. Gasparetto · V. Zanutto (✉)
DIEGM, University of Udine, Via delle Scienze 208, 33100 Udine, Italy
e-mail: vanni.zanutto@uniud.it

work has been done on modeling and control of such mechanisms. A comprehensive review of the work done in this area can be found in [1].

On the other hand, the experimental tests of control strategies for vibration reduction in flexible-link mechanisms (FLMs) give rise to some technical problems. FLMs are quite prone to mechanical failure, which occurs, for example, if strong torques warp the links as a consequence of an unsuitable control strategy. This also represents a potential safety risk for the operator. Replacing a broken link is a time-consuming task, since it is needed to attach a new strain gauge bridge to the beam, and to calibrate the strain gauge amplifier. Moreover the small differences often encountered between two links can reduce the reproducibility of the experiments.

One way to solve the problem can be found in Hardware-In-the-Loop (HIL) simulation. This technology allows the complete and right interaction of a real device (the controller) with a simulated one (the FLM).

In this case, the software that implements the dynamics of a flexible-link mechanism can be executed on a PC-based device and, through an I/O interface, the interaction with the real control system can be established. By using this method, many tests to get a suitable tuning of the control device can be done without involving the real mechanism, thus reducing the risk of mechanical failure as a result of an improper setup (Figs. 1 and 2). An HIL simulator is a valuable tool to give an evaluation of the performance of the control unit under investigation, in particular it can be used to test its real-time capability. Many modern control techniques,

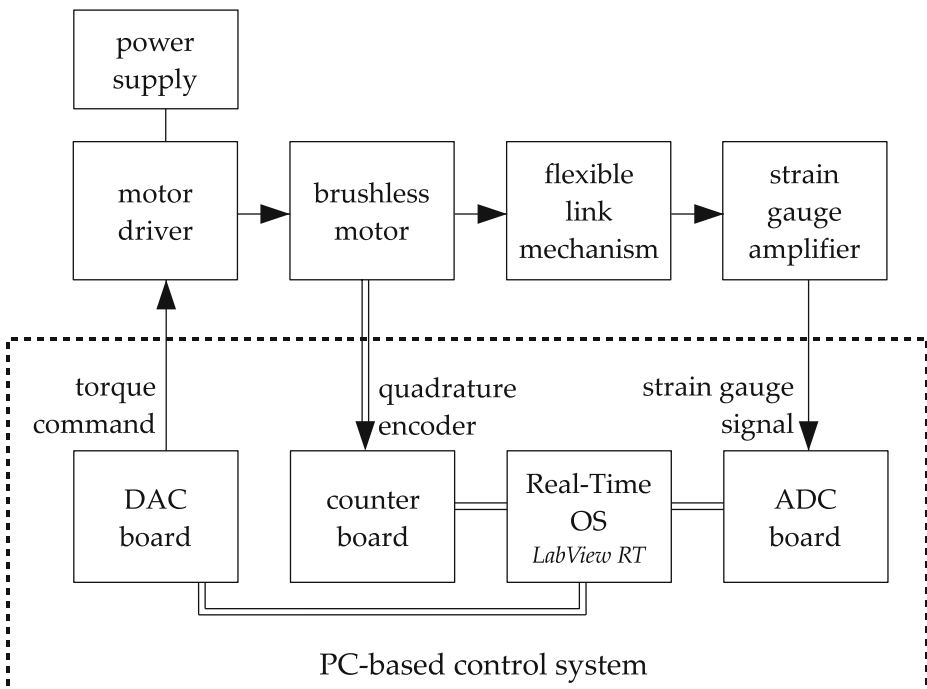


Fig. 1 Experimental tests: traditional approach

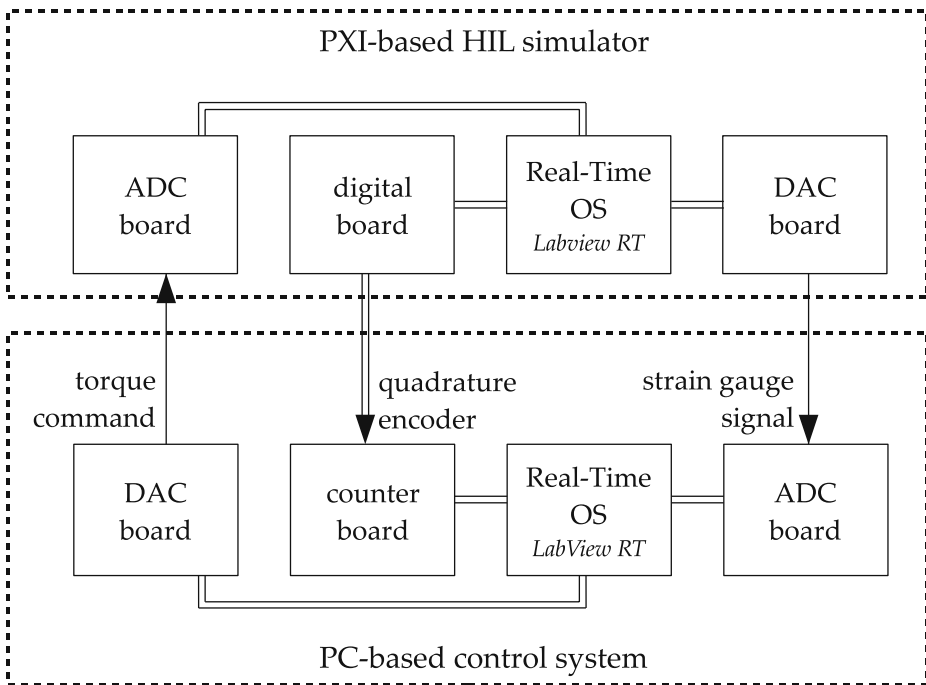


Fig. 2 Experimental tests: Hardware-In-the-Loop approach

such the very popular Model Predictive Control, are very demanding in term of computational power, so their Real-Time implementation can be very critical when high bandwidth and high complexity processes are involved. The proposed device can be used also to perform an in-depth analysis of the robustness of the control system under test. In many application, especially when model-based control is concerned, it is necessary to evaluate how the control unit would behave in the presence of mismatches between the modeled and the real plant. These test can be easily implemented with the aid of a Hardware-In-the-Loop simulator of the plant, simply by adding some parametric mismatches, nonlinearities, noise, etc. to the simulation model.

Among the advantages of the use of HIL simulators, lower implementation costs must be mentioned. Generally, and also in the considered case, the cost of the hardware needed to set-up a simulator like the proposed one is one fraction of the cost of building a real prototype. Moreover, it should be noticed that a careful design of an HIL test-bench allows to perform a seamless transition from the HIL to the traditional experimental setup, in the case that the HIL simulator has the very same physical connection to the control unit.

Other advantages of the HIL approach are:

- reproducibility of experiments
- the ability to perform tests which would otherwise be impossible, impractical and unsafe

- a shorter time required for experimental testing
- testing the effects of component faults
- long-term durability testing

Hardware-In-the-Loop technology is experiencing a wide diffusion in many industrial fields, in the wake of its early but successful introduction in the aerospace [2] and automotive [3] research areas. More recently many papers have been written on the subject of HIL simulator for mechatronic systems, such as [4, 5] on the use of HIL in machine tool design, [6] on the design of mobile robots and [7–9] on the analysis and synthesis of robotic systems. However, to the authors' best knowledge, there are no papers available in literature on the development or the use of Hardware-In-the-Loop simulators for mechanisms with link flexibility.

One requirement of the dynamic model used for the HIL simulation is the Real-Time capability, since it is necessary to make it interact with real-world signals, as the input and outputs of the control system are used in the feedback loop. This is a challenging problem, since the FLM dynamic model is both non-linear and high order. It involves large and badly conditioned matrices whose computation requires a large amount of resources [10]. Moreover, the structure of the model and its parameters make the dynamic equation ill-conditioned.

The proposed simulation can also be used for Real-Time SIL (Software-In-the-Loop) simulations [11, 12]. This strategy involves the interaction of two software devices, that in this case would simulate the mechanism and the control unit, respectively. This approach, while certainly valid, is less useful for our purposes than the HIL approach, since our target is to provide a full validation of the hardware implementation of the control system. In fact, unlike the SIL, the HIL technology allows to test the control unit as a whole system, composed by its hardware components (processor, memory, I/O devices) and its firmware.

Next section provides a brief explanation of the FLM dynamic model, while the main characteristics of the test bench are exposed in detail. In Section 3, some details of the Real-Time implementation will be introduced. In Section 4, the experimental results are presented. Here the validity of this approach is investigated by comparing the response of the HIL simulator with the response of the FLM to the same real controller. Two classical control strategy are tested: a usual PI controller and an Optimal LQY regulator.

Here two well-known control strategies are applied to the simplest flexible-link mechanism, namely the 1-link FLM, but the authors' aim is to address their future work to extending the capabilities of the proposed simulator to the 4-link FLM already analyzed in [13] and to use such a simulator to test the capabilities of the Model-Predictive Control proposed in [14, 15].

2 Dynamic Model of a Planar Flexible-link Mechanism

In this section the dynamic model of a flexible-link mechanism proposed by Giovagnoni [16] will be briefly outlined. This introduction is meant to give an insight of the model, which can be useful to better understand the complexity of the software implementation of the Hardware-In-the-Loop simulator. The choice of this formulation among the several proposed in the last 40 years has been motivated

mainly by the high grade of accuracy provided by this model, which has been proved several times: for example in [17–19].

Each flexible link belonging to the mechanism is divided into finite elements. The position of such elements are based on an Equivalent Rigid Link System (ERLS), as proposed by Chang and Hamilton [20] to express the coupling between the linkage global motion and vibrational motion. Referring to Fig. 3, the following vectors, calculated in the global reference frame $\{X, Y\}$, can be defined:

- \mathbf{r}_i and \mathbf{u}_i are the vectors of the nodal position and nodal displacement in the i th element of the ERLS, and of their elastic displacement
- \mathbf{p}_i is the position of a generic point inside the i th element
- \mathbf{q} is the vector of the generalized coordinates of the ERLS

Applying the principle of virtual work, the following relation can be stated:

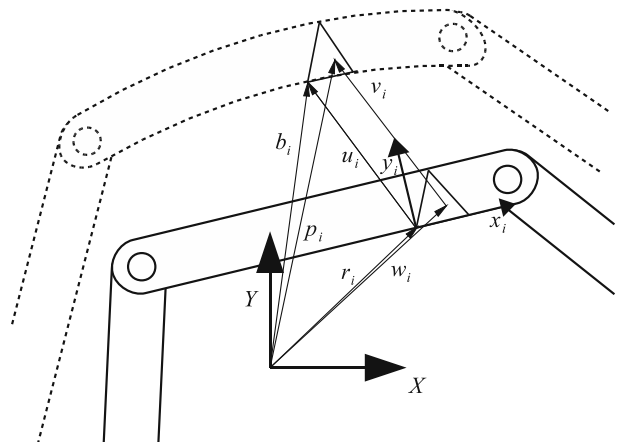
$$\begin{aligned} \sum_i \int_{V_i} \delta \mathbf{p}_i^T \ddot{\mathbf{p}}_i \rho_i dv + \sum_i \int_{V_i} \delta \epsilon_i^T \mathbf{D}_i \epsilon_i dv \\ = \sum_i \int_{V_i} \delta \mathbf{p}_i^T \mathbf{g} \rho_i dv + (\delta \mathbf{u}^T + \delta \mathbf{r}^T) \mathbf{F} \end{aligned} \quad (1)$$

ϵ_i , \mathbf{D}_i , ρ_i and $\delta \epsilon_i$ are, respectively, the strain vector, the stress-strain matrix, the mass density and the virtual strains of the i th link. \mathbf{F} is the vector of the external forces, including gravity, whose acceleration vector is \mathbf{g} . Equation 1 shows the virtual works of, respectively, inertia, elastic and external forces. From this equation, $\delta \mathbf{p}_i$ and $\ddot{\mathbf{p}}_i$ for a generic point in the i th element are:

$$\begin{aligned} \delta \mathbf{p}_i &= \mathbf{R}_i \mathbf{N}_i \mathbf{T}_i \delta \mathbf{r}_i \\ \ddot{\mathbf{p}}_i &= \mathbf{R}_i \mathbf{N}_i \mathbf{T}_i + 2(\dot{\mathbf{R}}_i \mathbf{N}_i \mathbf{T}_i + \mathbf{R}_i \dot{\mathbf{N}}_i \mathbf{T}_i) \dot{\mathbf{u}}_i \end{aligned} \quad (2)$$

where \mathbf{T}_i is a matrix that describes the transformation from the global-to-local reference frame of the i th element, \mathbf{R}_i is the local-to-global rotation matrix and \mathbf{N}_i is

Fig. 3 Kinematic definition of the ERLS



the shape function matrix. Taking $\mathbf{B}_i(x_i, y_i, z_i)$ as the strain-displacement matrix, the following relation holds:

$$\delta \epsilon_i = \mathbf{B}_i \delta \mathbf{T}_i \mathbf{u}_i + \mathbf{B}_i \mathbf{T}_i \delta \mathbf{u}_i \quad (3)$$

Since the nodal elastic virtual displacements ($\delta \mathbf{u}$) and nodal virtual displacements of the ERLS ($\delta \mathbf{r}$) are independent from each other, the resulting equation describing the motion of the system is:

$$\begin{bmatrix} \mathbf{M} & \mathbf{MS} \\ \mathbf{S}^T \mathbf{M} & \mathbf{S}^T \mathbf{MS} \end{bmatrix} \begin{bmatrix} \ddot{\mathbf{u}} \\ \ddot{\mathbf{q}} \end{bmatrix} = \begin{bmatrix} \mathbf{f} \\ \mathbf{S}^T \mathbf{f} \end{bmatrix} \quad (4)$$

\mathbf{M} is the mass matrix of the whole system and \mathbf{S} is the sensitivity matrix for all the nodes. Vector $\mathbf{F} = \mathbf{F}(\mathbf{u}, \dot{\mathbf{u}}, \mathbf{q}, \dot{\mathbf{q}})$ takes into account all the forces affecting the system, including the force of gravity and the friction. The friction acting on the shaft of the motor is modeled as Coulomb friction. The coefficient of friction has been evaluated experimentally, and has been implemented as in [21] in order to avoid numerical problems during the solution of the ODE that describe the system dynamics. The damping of elastic vibration is modeled using Rayleigh damping, introducing it to the right-hand side of Eq. 4 yields:

$$\begin{bmatrix} \mathbf{f} \\ \mathbf{S}^T \mathbf{f} \end{bmatrix} = \begin{bmatrix} -2\mathbf{M}_G - \alpha \mathbf{M} - \beta \mathbf{K} & -\mathbf{M}\dot{\mathbf{S}} & -\mathbf{K} \\ \mathbf{S}^T(-2\mathbf{M}_G - \alpha \mathbf{M}) & -\mathbf{S}^T \mathbf{M}\dot{\mathbf{S}} & 0 \end{bmatrix} \begin{bmatrix} \dot{\mathbf{u}} \\ \dot{\mathbf{q}} \\ \mathbf{u} \end{bmatrix} + \begin{bmatrix} \mathbf{M} & \mathbf{I} \\ \mathbf{S}^T \mathbf{M} & \mathbf{S}^T \end{bmatrix} \begin{bmatrix} \mathbf{g} \\ \mathbf{F} \end{bmatrix} \quad (5)$$

Matrix \mathbf{M}_G accounts for the Coriolis contribution, while \mathbf{K} is the stiffness matrix of the whole system. α and β are the two Rayleigh damping coefficients. The system in Eqs. 4 and 5 can be made solvable by forcing to zero as many elastic displacements as there are generalized coordinates, and in this way the ERLS position is defined univocally [16]. Finally, after removing the displacement forced to zero from Eqs. 4 and 5 one obtains:

$$\begin{bmatrix} \mathbf{M}_{in} & (\mathbf{MS})_{in} \\ (\mathbf{S}^T \mathbf{M})_{in} & \mathbf{S}^T \mathbf{MS} \end{bmatrix} \begin{bmatrix} \ddot{\mathbf{u}}_{in} \\ \ddot{\mathbf{q}} \end{bmatrix} = \begin{bmatrix} \mathbf{f}_{in} \\ \mathbf{S}^T \mathbf{f}_{in} \end{bmatrix} \quad (6)$$

2.1 Reference Mechanism

The mechanism for the HIL simulation is a flexible-link manipulator. The link is a square-section metal rod actuated by a brushless AC motor. It can swing in the vertical plane and its rigid configuration depends on the angular position q .

Evidence of exhaustive experimental tests allows to choose the suitable number of finite elements needed to describe the mechanism's dynamics accurately. The main frequencies of the flexible rod have been inferred by analyzing the spectrum of the vibration when the rod is excited by tapping its end with a steel hammer. This experimental data is then compared with the response of the HIL simulator to the same stimulus. Such conditions can be reproduced by locking the rotation of the rigid degree of freedom q and providing a sequence of impulsive forces to the last node of the FLM (Fig. 4).

Fig. 4 The mechanisms used for experimental tests



Figure 5 shows the results of this comparison. The black line draws the FFT of the strain-gauge signal, acquired through a Hottinger Baldwin Messtechnik KWS 3073 amplifier. The gray line shows the FFT of the corresponding displacement of the HIL simulator, for the node at the mid-span of the link.

Experimental tests allow to choose the correct number of finite elements and show that only four elements can describe the overall dynamics of the link with good accuracy, as proved in Fig. 5. The HIL simulator can take into account, with negligible errors, the first three modes of the real mechanism (namely 4.5, 28, 81 Hz) and, with lesser but still sufficient precision, the modes at 167 and 274 Hz.

It should be pointed out that the modes of high order are less important for the description of the elasto-dynamics of FLM, since they have a very fast decay-time. As such, the resulting nodal displacement is a vector of 12 elements:

$$\mathbf{u} = [u_1 \ u_2 \ u_3 \ \dots \ u_{11} \ u_{12}]' \quad (7)$$

Fig. 5 Frequency spectrum of strain signal: comparison between experimental results and HIL simulation

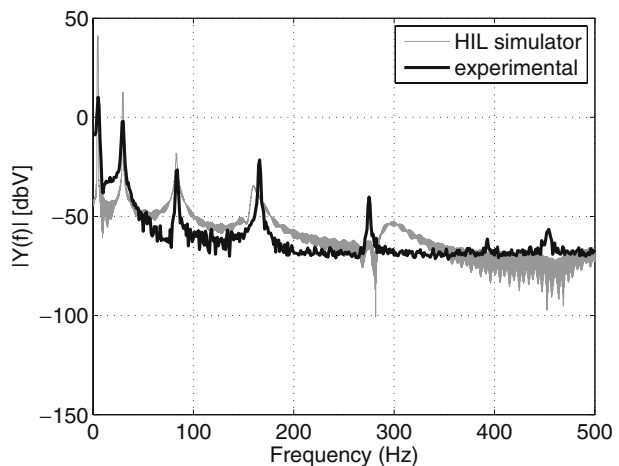
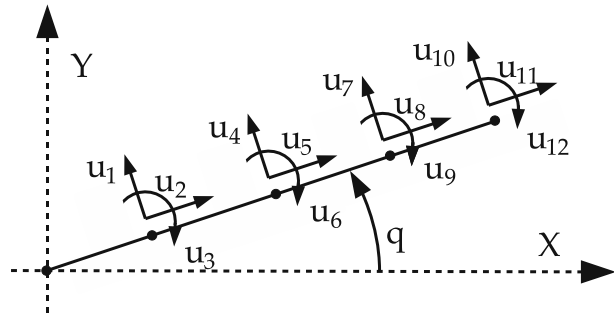


Fig. 6 Finite-element discretization: nodal displacements



The strain measured can be directly linked to the angular displacement u_6 , located at the third node, as it can be seen in Fig. 6. From this choice of finite elements, the state vector \mathbf{x} in Eq. 5 has 26 components, and the size of the mass matrix in Eq. 6 is 26×26 .

The accuracy of the Hardware-In-the-Loop simulator has been increased including the non-ideal behavior of the real plant. Additive white gaussian noise have been added to both the simulated strain-gauge signal and to the simulated signal of the encoder. The contribution on strain-gauge signal is crucial, since this kind of signal is affected by large amount of noise, due to the strain-gauge amplifier high gain. Moreover this signal is highly affected by the noise irradiated by the motor driver power supply. The gain of the simulated strain gauge amplifier has been set to 200, meaning that an elastic displacement of 0.01 radians would produce an analog signal with 2 Volts amplitude.

The dynamics of the motor driver and of the actuator have been modeled as a first order low-pass filter with time constant τ_m , and the moment of inertia of the motor J_m has also been included. Such values, which are reported in Table 2, have been evaluated experimentally to refine the accuracy of the simulated dynamic model.

The two Rayleigh damping coefficients listed in Table 1 have been also determined experimentally, by comparing the decay time of the vibration of the real mechanism with the one of the HIL simulator (Table 2).

Table 1 Structural and dynamics characteristics of the flexible rod

| | Symbol | Value |
|----------------------------------|----------|--|
| Young's modulus | E | $230 \cdot 10^9$ [Pa] |
| Flexural stiffness | EJ | 191.67 [Nm ⁴] |
| Beam width | a | $1 \cdot 10^{-2}$ [m] |
| Beam thickness | b | $1 \cdot 10^{-2}$ [m] |
| Mass/unit length | m | 0.7880 [kg/m] |
| Flexible Link length | l | 1.5 [m] |
| Strain sensor position | s | 0.75 [m] |
| First Rayleigh damping constant | α | $4.5 \cdot 10^{-1}$ [s ⁻¹] |
| Second Rayleigh damping constant | β | $4.2 \cdot 10^{-5}$ [s ⁻¹] |

Table 2 Dynamic characteristics of the actuator

| | Symbol | Value |
|-----------------------------------|----------|-----------------------------|
| Motor time constant | τ_m | 3 [ms] |
| Motor shaft inertia | J_m | 0.0021 [kg m ²] |
| Coulomb friction coefficient | μ | 0.1 |
| Driver torque analog command gain | G_d | 0.4 [Nm]/[V] |

3 HIL Implementation

The goal of the Hardware-In-the-Loop simulator is to make the real controller and the simulated model interact with each other, without any need of change on the structure and/or the tuning of the controller. As such, the dynamic model must meet two main requirements: (a) high accuracy (b) real-time (RT) capability.

The accuracy allows to mask the virtual model to the controller and, undoubtedly, allows to make the experiments consistent. The dynamic model described above has been investigated by the same authors and its accuracy has been demonstrated in recent papers by comparing the results of several experimental tests with the corresponding simulation's results [22].

The need for the RT capacity arises from the mentioned interaction between real and simulated signals. This requires the dynamic model running on the RT target must have a constant updating frequency to allow the correct synchronization among the signals. These constraints ask for some algebraic manipulations on the dynamic model (Fig. 7).

Real-Time
controller

HIL
simulator

**Fig. 7** The HIL test bench: PXI-based simulator and real-time controller

Equation 6 can be rewritten as:

$$\begin{bmatrix} \mathbf{M} & \mathbf{M}\mathbf{S} & \mathbf{0} & \mathbf{0} \\ \mathbf{S}^T\mathbf{M} & \mathbf{S}^T\mathbf{M}\mathbf{S} & \mathbf{0} & \mathbf{0} \\ \mathbf{0} & \mathbf{0} & \mathbf{I} & \mathbf{0} \\ \mathbf{0} & \mathbf{0} & \mathbf{0} & \mathbf{I} \end{bmatrix} \begin{bmatrix} \ddot{\mathbf{u}} \\ \ddot{\mathbf{q}} \\ \dot{\mathbf{u}} \\ \dot{\mathbf{q}} \end{bmatrix} = \begin{bmatrix} \mathbf{M} & \mathbf{I} \\ \mathbf{S}^T\mathbf{M} & \mathbf{S}^T \end{bmatrix} \begin{bmatrix} \mathbf{g} \\ \mathbf{F} \end{bmatrix} + \begin{bmatrix} -2\mathbf{M}_G - \alpha\mathbf{M} - \beta\mathbf{K} & -\mathbf{M}\dot{\mathbf{S}} & -\mathbf{K} & \mathbf{0} \\ \mathbf{S}^T(-2\mathbf{M}_G - \alpha\mathbf{M}) & -\mathbf{S}^T\mathbf{M}\dot{\mathbf{S}} & \mathbf{0} & \mathbf{0} \\ \mathbf{I} & \mathbf{0} & \mathbf{0} & \mathbf{0} \\ \mathbf{0} & \mathbf{I} & \mathbf{0} & \mathbf{0} \end{bmatrix} \begin{bmatrix} \dot{\mathbf{u}} \\ \dot{\mathbf{q}} \\ \mathbf{u} \\ \mathbf{q} \end{bmatrix}$$

or, in a more compact form:

$$\tilde{\mathbf{M}}(\mathbf{x}, t)\dot{\mathbf{x}} = \Phi(\mathbf{x}, \mathbf{F}, t) \quad (8)$$

where:

$$\mathbf{x} = [\dot{\mathbf{u}}, \dot{\mathbf{q}}, \mathbf{u}, \mathbf{q}]^T$$

and

$$\Phi(\mathbf{x}, \mathbf{F}, t) = \begin{bmatrix} \mathbf{M} & \mathbf{I} \\ \mathbf{S}^T\mathbf{M} & \mathbf{S}^T \\ \mathbf{0} & \mathbf{0} \\ \mathbf{0} & \mathbf{0} \end{bmatrix} \begin{bmatrix} \mathbf{g} \\ \mathbf{F} \end{bmatrix} + \begin{bmatrix} -2\mathbf{M}_G - \alpha\mathbf{M} - \beta\mathbf{K} & -\mathbf{M}\dot{\mathbf{S}} & -\mathbf{K} & \mathbf{0} \\ \mathbf{S}^T(-2\mathbf{M}_G - \alpha\mathbf{M}) & -\mathbf{S}^T\mathbf{M}\dot{\mathbf{S}} & \mathbf{0} & \mathbf{0} \\ \mathbf{I} & \mathbf{0} & \mathbf{0} & \mathbf{0} \\ \mathbf{0} & \mathbf{I} & \mathbf{0} & \mathbf{0} \end{bmatrix} \mathbf{x}$$

$$\tilde{\mathbf{M}}(\mathbf{x}, t) = \begin{bmatrix} \mathbf{M} & \mathbf{M}\mathbf{S} & \mathbf{0} & \mathbf{0} \\ \mathbf{S}^T\mathbf{M} & \mathbf{S}^T\mathbf{M}\mathbf{S} & \mathbf{0} & \mathbf{0} \\ \mathbf{0} & \mathbf{0} & \mathbf{I} & \mathbf{0} \\ \mathbf{0} & \mathbf{0} & \mathbf{0} & \mathbf{I} \end{bmatrix}$$

From Eq. 8, it can be seen that the updating equation of the dynamic system involves a large, non-linear and time-dependent matrix, $\tilde{\mathbf{M}}(\mathbf{x}, t)$, which needs to be inverted at every iteration.

$$\dot{\mathbf{x}} = \tilde{\mathbf{M}}(\mathbf{x}, t)^{-1}\Phi(\mathbf{x}, \mathbf{F}, t) \quad (9)$$

It should be point out that, owing to the specific choice of the constraints on the flexible displacements \mathbf{u} , the matrix $\tilde{\mathbf{M}}$ is always nonsingular.

To speed up the computation of $\dot{\mathbf{x}}$ and improve the updating time, it is necessary to make explicit the vector $\dot{\mathbf{x}}$, by computing its components algebraically. This operation can be done off-line and improves the updating time drastically, since the computation of Eq. 9 becomes a mere numerical substitution during the run-time operations. The main drawback of this approach is that a large amount of memory is required to memorize all the components of the vector.

An optimized C-code routine corresponding to Eq. 9 further improves the real-time (or even faster-than-real-time) capacity.

The RT simulation of the whole system, including sensors, actuators and drivers runs on a National Instruments PXI device. It integrates a standard PC-based CPU with a high performance I/O board, so it is well suited for both control and measurement applications.

In particular, the HIL simulator has been implemented on a 1042Q PXI chassis with a PXI-8110 controller, a PXI-6259 analog I/O board and a PXI-6602 counter board, all made by National Instruments®.

The dynamic equation, originally written in C language, can be easily included in a LabVIEW RT project.

In order to evaluate the maximum refresh frequency of the HIL simulator, a large number of tests has been done. The aim was at evaluation of the maximum time required for the computation of Eq. 9.

The results show that the mean time required is $\bar{T} = 0.61831428$ ms, evaluated with the precision of 4×10^{-8} s. As a consequence, the model's refresh frequency for all the experimental tests presented in this paper has been set to 1 kHz. This sampling frequency is sufficient to describe with a good accuracy all the first seven modes of vibration of the flexible link.

4 Experimental Validation of the HIL Simulator

A set of experimental tests has been conducted to prove the effectiveness of the HIL simulator. In particular, the simulator has been validated by using classical controllers while the comparison between the open-loop responses of the real and the simulated plant is necessary missing. This depends on the gravity force that makes unstable the plant.

It must be pointed out that, for each experimental test, the same (real) controller has been used both for the real mechanism and the simulated one, without any change on its setup.

In Section 4.1 the simulator is validated by comparing the step response of the real and the simulated mechanism, when the controller implements a simple PI regulator. In Section 4.2 the same comparison is done by using a LQY regulator.

4.1 Validation with PI Closed-loop Position Control

In this section, the real controller implements a simple PI regulator with a feed-forward gravity-compensation action. The block diagram of the control system is depicted in Fig. 8.

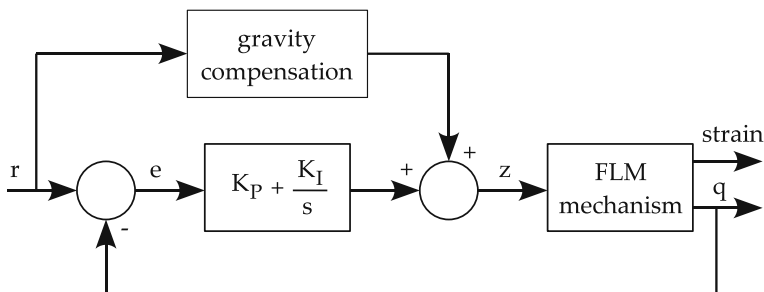


Fig. 8 PI position control: control diagram

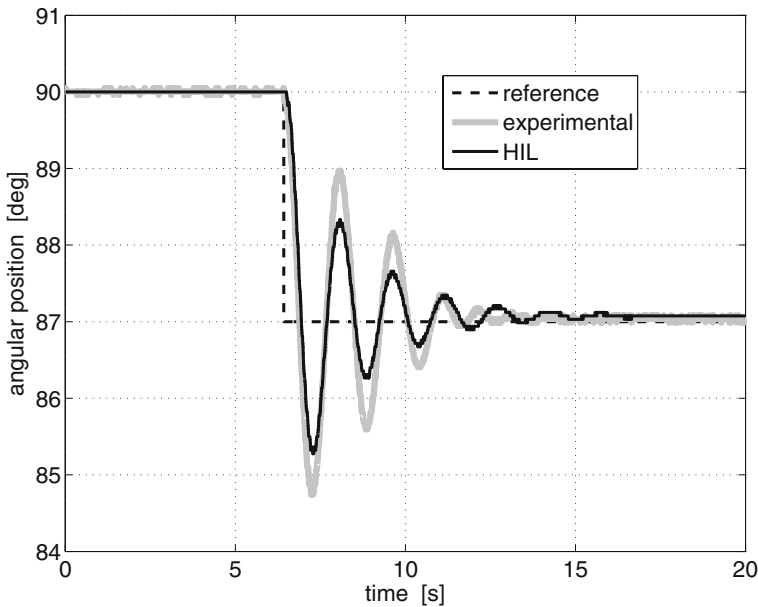


Fig. 9 PI position control: experimental validation of the angular position closed-loop response

Figure 9 shows the comparison between the angular position of the real mechanism and the HIL simulator. The reference signal is a 3° wide step. It can be seen that the two positions are almost equal.

In Figs. 10 and 11 the torque commands and the strain gauge signals are compared, respectively.

In Fig. 10, the small difference between the real and the simulated signals is due to the approximation of the link curvature with the nodal displacement u_6 .

All the figures demonstrate the effectiveness of the HIL simulator. As such, it can simulate with a good accuracy the behavior of the real mechanism.

A PID control system might have been used as well, but the choice of a simple PI control has been motivated for its damping properties: a less damped system is more demanding on the accuracy of the HIL test bench.

4.2 Validation with LQ Closed-loop Position and Vibration Control

In this section a further proof of the accuracy of the Hardware-In-the-Loop simulator is given, by comparing with each other the responses of the real and the HIL-simulated plant by using a LQ position-vibration controller with an integral action. A graphic representation of the control's loop structure is shown in Fig. 12.

Owing to the space constraints of this paper, just a basic overview of this controller will be given. A complete explanation of this controller can be found in [23].

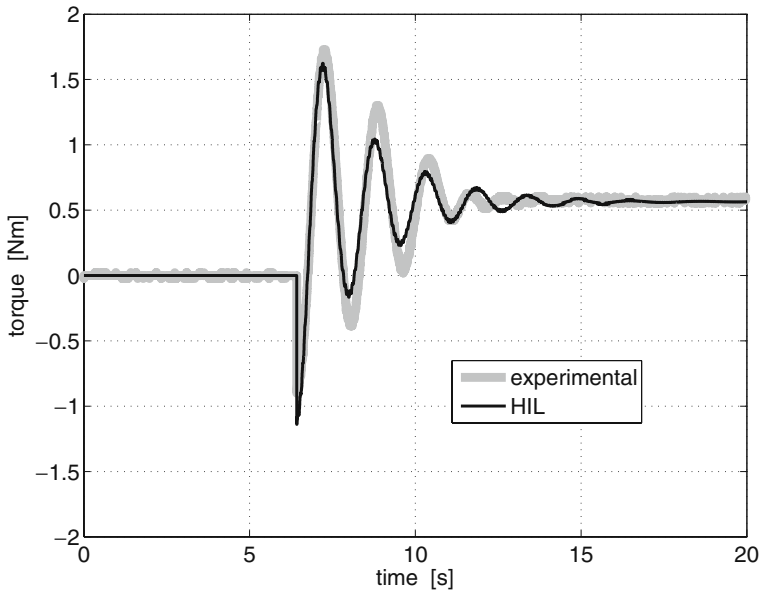


Fig. 10 PI position control: experimental validation of the torque closed-loop response

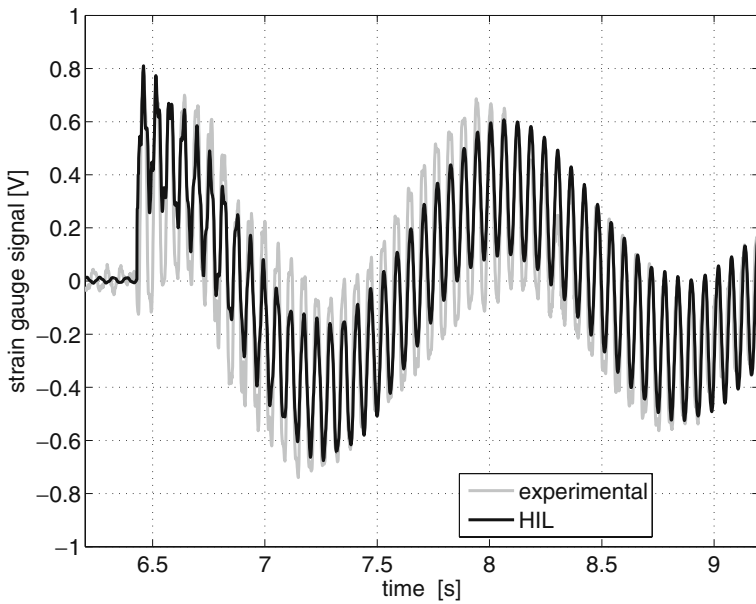


Fig. 11 PID position control: experimental validation of the strain gauge signal closed-loop response—detailed view of the transient

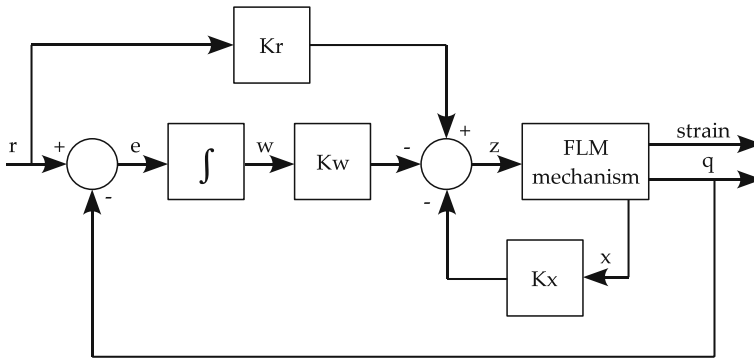


Fig. 12 LQY with integral action position and vibration control: control diagram

The design of such a controller is based on a linear state-space model of the FML which has been obtained through a classical linearization procedure of Eq. 5. The resulting state-space model can be written as:

$$\begin{cases} \dot{\mathbf{x}}(t) = \mathbf{A}\mathbf{x}(t) + \mathbf{B}\mathbf{z}(t) \\ \mathbf{y}(t) = \mathbf{C}\mathbf{x}(t) \end{cases} \quad (10)$$

where $\mathbf{A} \in \mathbb{R}^{26} \times \mathbb{R}^{26}$, $\mathbf{B} \in \mathbb{R}^{26} \times \mathbb{R}^1$, $\mathbf{C} \in \mathbb{R}^2 \times \mathbb{R}^{26}$ are time-invariant matrices.

In order to provide an integral action to the controller, the state-space model must be augmented. The tracking error can be defined so that its time derivative obeys the following differential equation:

$$\dot{\mathbf{w}} = \mathbf{r}(t) - \mathbf{y}(t) = \mathbf{r}(t) - \mathbf{C}\mathbf{x}(t) \quad (11)$$

where $\mathbf{r}(t)$ is the desired trajectory that the plant output $\mathbf{y}(t)$ should follow. In this way $\mathbf{w}(t)$ is the integral of the tracking error. An augmented state vector $\hat{\mathbf{x}}$ can be defined such as: $\hat{\mathbf{x}} = \begin{bmatrix} \mathbf{x} \\ \mathbf{w} \end{bmatrix}$, then the augmented state equation is:

$$\dot{\hat{\mathbf{x}}}(t) = \underbrace{\begin{bmatrix} \mathbf{A} & 0 \\ -\mathbf{C} & 0 \end{bmatrix}}_{\hat{\mathbf{A}}} \hat{\mathbf{x}} + \underbrace{\begin{bmatrix} \mathbf{B} \\ 0 \end{bmatrix}}_{\hat{\mathbf{B}}} \mathbf{z} + \underbrace{\begin{bmatrix} 0 \\ \mathbf{r} \end{bmatrix}}_{\mathbf{d}} \quad (12)$$

while the augmented output equation is:

$$\mathbf{y} = \underbrace{[\mathbf{C} \ 0]}_{\hat{\mathbf{C}}} \hat{\mathbf{x}} \quad (13)$$

The LQY controller calculates the optimal control sequence $\tau(t)$ which minimizes the performance index J , defined as:

$$J = \frac{1}{2} \int_0^\infty \left\{ (\mathbf{y} - \mathbf{r})^T \mathbf{Q}_y (\mathbf{y} - \mathbf{r}) + \mathbf{w}^T \mathbf{Q}_w \mathbf{w} + \mathbf{z}^T \mathbf{R} \mathbf{z} \right\} dt \quad (14)$$

The first term inside the integral minimizes the absolute value of the tracking error of free coordinate q and the elastic displacement, whereas the second takes into account the absolute value of integral error of q . The last one minimizes the system input, namely the torque applied to the link.

\mathbf{Q}_y is a diagonal matrix of weights, while \mathbf{Q}_w and \mathbf{R} are simple scalar values. The value of the control variable can be found as:

$$z(t) = -\mathbf{K}_x \mathbf{x} - \mathbf{K}_w w + \mathbf{K}_r \mathbf{r} \quad (15)$$

where the optimal value of the gain matrices \mathbf{K}_x , \mathbf{K}_w , \mathbf{K}_r are found through the solution of the algebraic Riccati equation.

The control strategy explained above can be applied only when a measure of the whole state \mathbf{x} is available. In this application, there are only two measured values, so that a state observer must be used. Here a standard Kalman asymptotic estimator has been chosen. An estimation of $\mathbf{x}(k)$ and $\mathbf{x}_m(k)$ (where $\mathbf{x}(k)$ is the state of the plant model and $\mathbf{x}_m(k)$ is the state of the measurement noise model) can be computed from the measured output $\mathbf{y}_m(k)$ through:

$$\begin{aligned} \begin{bmatrix} \hat{\mathbf{x}}(k|k) \\ \hat{\mathbf{x}}_m(k|k) \end{bmatrix} &= \begin{bmatrix} \hat{\mathbf{x}}(k|k-1) \\ \hat{\mathbf{x}}_m(k|k-1) \end{bmatrix} + \mathbf{L}(\mathbf{y}_m(k) - \hat{\mathbf{y}}_m(k)) \\ \begin{bmatrix} \hat{\mathbf{x}}(k+1|k) \\ \hat{\mathbf{x}}_m(k+1|k) \end{bmatrix} &= \begin{bmatrix} \mathbf{A}\hat{\mathbf{x}}(k|k) + \mathbf{B}\mathbf{z}(k) \\ \tilde{\mathbf{A}}\hat{\mathbf{x}}_m(k|k) \end{bmatrix} \\ \hat{\mathbf{y}}_m(k) &= \mathbf{C}_m \hat{\mathbf{x}}_m(k|k-1) \end{aligned} \quad (16)$$

The gain matrix \mathbf{L} is designed by using Kalman filtering techniques, see [24].

The response of the HIL simulator and of the mechanism when the LQ position and vibration control is used are reported in Figs. 13, 14, 15 and in Figs. 16, 17, 18. Two different tunings of the control system have been used to show how the HIL simulator can respond to different control parameters.

4.2.1 LQ Control: Experimental Validation

The first experimental validation using the LQ optimal control with integral action is done using the following tuning parameters: $\mathbf{Q}_y = \begin{bmatrix} 1000 & 0 \\ 0 & 50 \end{bmatrix}$ and $\mathbf{Q}_w = 100$.

The initial position of the mechanism is 90° , and the reference signal is a step that moves from 90° – 94° . The response of the mechanism and the HIL simulator are compared in Fig. 13. As it can be seen, the responses are very similar each other. The small discrepancies are the result of the limited accuracy of the brushless motor torque control. A more accurate comparison would require to effectively measure the torque produced by the actuator.

The values of the torque computed by the real-time control system are compared in Fig. 14. Again, the accuracy of the HIL simulator is confirmed by the likeness of the two torque profiles.

The accuracy of the proposed Hardware-In-the-Loop simulator in terms of vibration response is shown in Fig. 15.

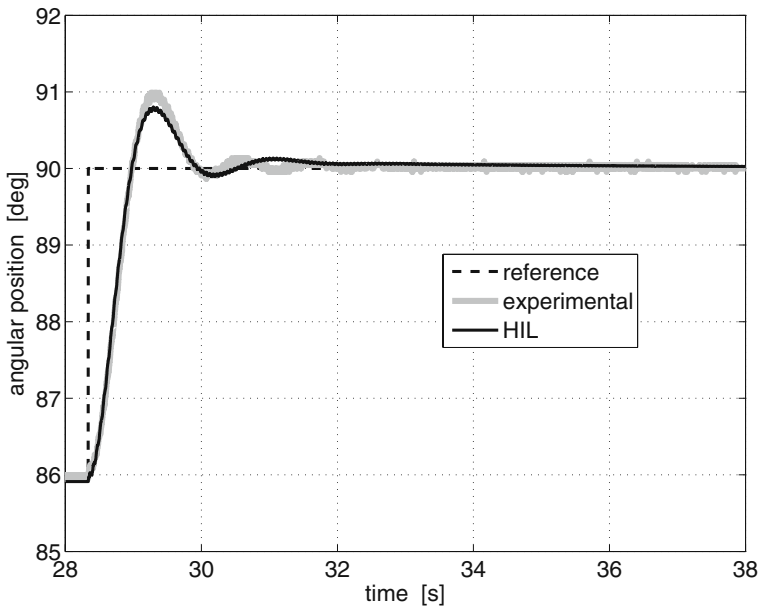


Fig. 13 Optimal control: experimental validation of the angular position closed-loop response

It should be noted that the LQ controller needs the HIL simulator have a higher level of accuracy comparing to the requirements of the previous PI control, since it also relies on the elastic displacement for the computation of the control action.

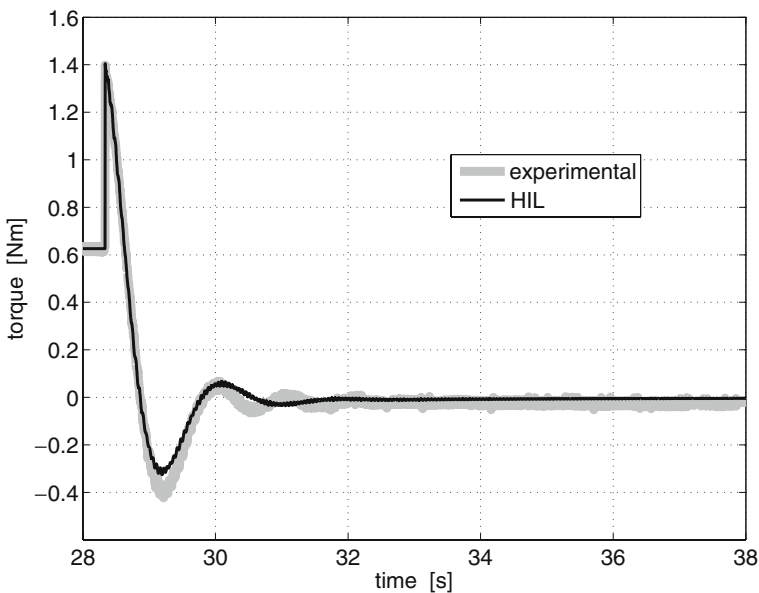


Fig. 14 Optimal control: experimental validation of the torque closed-loop response

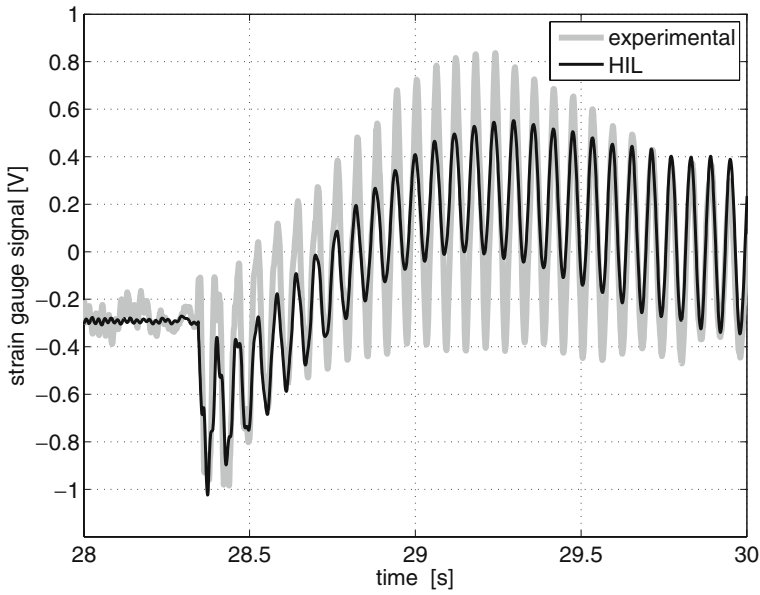


Fig. 15 Optimal control: experimental validation of the strain gauge signal closed-loop response—detailed view of transient

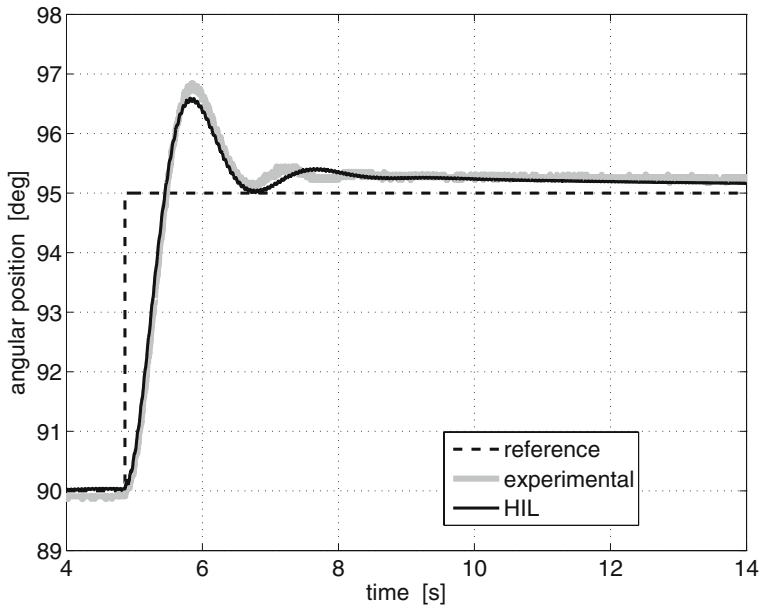


Fig. 16 Optimal control: experimental validation of the angular position closed-loop response

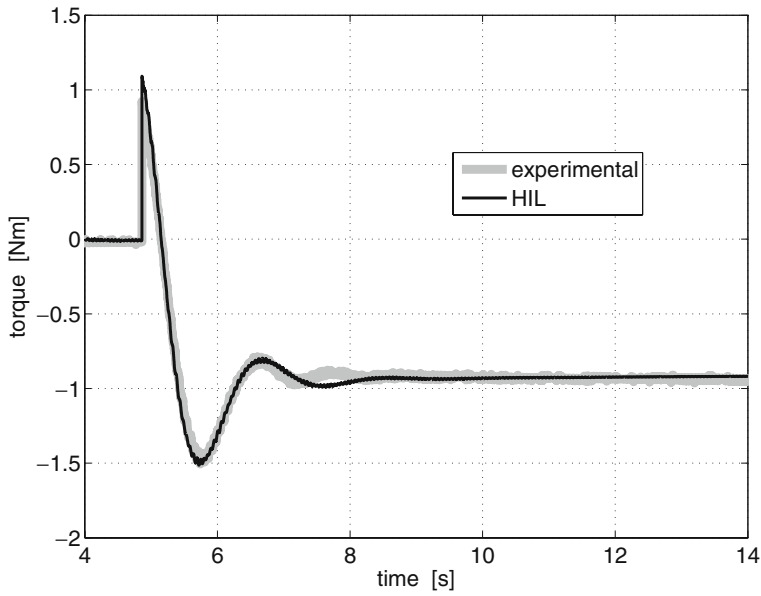


Fig. 17 Optimal control: experimental validation of the torque closed-loop response

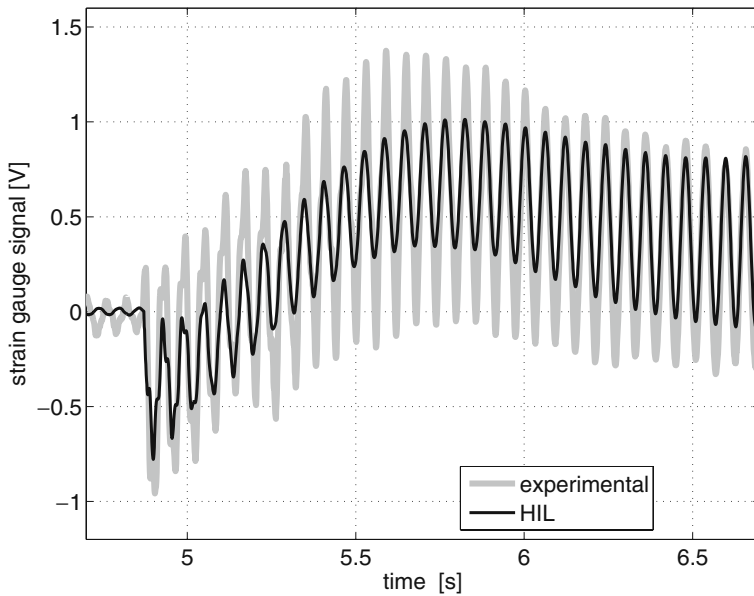


Fig. 18 Optimal control: experimental validation of the strain gauge signal closed-loop response—detailed view of transient

The second experimental validation is done by setting the following parameters:

$$\mathbf{Q}_y = \begin{bmatrix} 500 & 0 \\ 0 & 100 \end{bmatrix} \text{ and } \mathbf{Q}_w = 50.$$

As it can be seen from Figs. 16–18 the likeness of the two responses exhibited in the previous test is kept at the same level also after altering the tuning of the control system.

5 Conclusion

This paper presents a HIL simulator for flexible-link manipulators. The HIL technique allows to perform several experiments on a real controller without involving the actual mechanism, thereby increasing the safety, reducing the time involved in the control tuning and eliminating any mechanical failure. Once the controller has been set up correctly, it can be directly connected to the physical plant without any further adjustment. Eventually, the real tests can be conducted in a usual way. However, the risk due to an incorrect controller action has been drastically reduced. The main problem of the HIL simulator for flexible-link manipulator concerns the real-time capability, since the real signals of the controller must interact with the simulated signals of the plant. Therefore, the differential equations governing the plant must be quickly integrated and solved. A fast and effective way to compute the dynamic model of planar flexible-link mechanisms has been presented in this work. The accuracy and the effectiveness of the simulator have been demonstrated through experimental evidence and by using different control structures. Future works will consider more complex flexible-link mechanisms to which apply advanced control structures for vibration reduction, as those presented in previous works by the same authors, but only with simulated results.

References

1. Dwivedy, A.K., Eberhard, P.: Dynamical analysis of flexible manipulators, a literature review. *Mech. Mach. Theory* **41**(7), 749–777 (2006)
2. Leitner, J.: Space technology transition using hardware in the loop simulation. In: *Proc. 1996 Aerospace Applications Conference*, **2**, 303–311
3. Hanselman, H.: Hardware-in-the-loop simulation testing and its integration into a CACSD toolset. In: *Proc. IEEE International Symposium on Computer-Aided Control System Design*, 15–18 September 1996
4. Pritshow, G., Röck, S.: Hardware in the loop simulation of machine tools. *CIRP Ann.* **53**(1), 259–298 (2004)
5. Stoeppler, G., Menzel, T., Douglas, S.: Hardware-in-the-loop simulation of machine tools and manufacturing systems. *Comput. Control Eng. J.* **16**(1), 10–15 (2005)
6. Hu, X.: Applying robot-in-the-loop simulation to mobile robot systems. In: *Proc. 12th International Conference on Advanced Robotics ICAR* (2005)
7. Aghili, F., Piedboeuf, J.C.: Contact dynamics emulation for hardware-in-loop simulation of robots interacting with environment. In: *Proc. ICRA '02. IEEE International Conference on Robotics and Automation*
8. Chabira, R., Emami, M.R.: Concurrent design of robot manipulators using hardware-in-the-loop simulation. In: *Proc. 2008 IEEE International Conference on Technologies for Practical Robot Applications (TePRA)*, Massachusetts, USA (2008)
9. Martin A., Scot, E., Emami, M.R.: Design and development of robotic hardware-in-the-loop simulation. In: *Proc. 9th ICAR International Conference on Control, Automation, Robotics and Vision*, vol. 1, no. 6 (2006)

10. Wasfy, T.M., Noor, A.K.: Computational strategies for flexible multibody systems. *Appl. Mech. Rev.* **56**(6), 553–613 (2003)
11. Bringmann E., Kramer A.: Model-based testing of automotive systems. 2008 1st IEEE International Conference on Software Testing, Verification, and Validation, pp. 485–493 (2008)
12. Isermann, R., Schaffnit, J., Sinsel, S.: Hardware-in-the-loop simulation for the design and testing of engine-control systems. *Control Eng. Pract.* **7**(5), 643–653 (1999)
13. Boscariol, P., Gasparetto, A., Zanotto, V.: Active position and vibration control of a flexible links mechanism using model-based predictive control. *J. Dyn. Syst. Meas. Control* **132**(1), 014506 (2010)
14. Boscariol, P., Gasparetto, A., Zanotto, V.: Model predictive control of a flexible links mechanism. *J. Intell. Robot. Syst.* **58**(2), 125–147 (2010)
15. Boscariol, P., Gasparetto, A., Zanotto, V.: Vibrations reduction in a flexible link mechanism through the synthesis of an MPC controller. In: *Proc: IEEE International Conference on Mechatronics ICM 2009, Malaga, Spain* (2009)
16. Giovagnoni M.: A numerical and experimental analysis of a chain of flexible bodies. *ASME J. Dyn. Syst. Meas. Control* **113**, 73–80 (1994)
17. Trevisani, A., Valcher, M.E.: An energy-based adaptive control design technique for multibody-mechanisms wit flexible-links. *IEEE/ASME Trans. Mechatron.* **10**(5), 571–580 (2005)
18. Gasparetto A., Zanotto, V.: Vibration reduction in a flexible-link mechanism through synthesis of an optimal controller. *Meccanica* **41**(6), 611–622 (2006)
19. Caracciolo, R., Richiedei, D., Trevisani, A.: Design and experimental validation of piecewise-linear state observers for flexible link mechanism. *Meccanica* **41**(6), 623–637 (2006)
20. Chang, L.W., Hamilton, J.F.: The kinematics of robotic manipulators with flexible links using an equivalent rigid link system (ERLS) model. *ASME J. Dyn. Syst. Meas. Control* **113**, 48–53 (1991)
21. Mostaghel N., Davis T.: Representation of coulomb friction for dynamic analysis. *Earthq. Eng. Struct. Dyn.* **26**, 541–548 (1997)
22. Gasparetto, A.: On the modeling of flexible-link planar mechanism: experimental validation of an accurate dynamic model. *ASME J. Dyn. Syst. Meas. Control* **126**(2), 365–375 (2004)
23. Naidu D.S.: *Optimal control systems*. CRC (2003)
24. Franklin, F.G., Powell, F.G., Workman, M.L.: *Digital control of dynamic systems*, 2nd edn. Addison Wesley (1990)